COSMIC AND SUBATOMIC PHYSICS REPORT
LUIP 8512
JANUARY 1986
(LUNFD6/(NFFK-7065)1-31(1986))
ISSN 0348-9329

MONTE-CARLO SIMULATIONS OF ANOMALON EXPERIMENTS

B Norén och B Jakobsson
Department of Physics
University of Lund
Sweden

Cosmic and Subatomic Physics
University of Lund
Sölvegatan 14
S-223 62 Lund, Sweden

Monte-Carlo Simulations of Anomalon Experiments

B. Norén and B. Jakobsson
Department of Physics
University of Lund
Sweden

Computer simulations of low statistics track detector heavy ion collision experiments on projectile fragmentation are presented. We find a non-negligible probability to obtain the recently observed anomalous fragmentation component also with normal fragmentation processes. We discuss the significance of the expected mean-free-path behaviour when an anomalous component is included.

1. Introduction

Nuclear emulsion experiments [1-6], bubble chamber experiments [7-8], plastic detector experiments [9] and radiochemical experiments [10] have reported on an anomalous fragmentation component in heavy ion reactions with an extremely large reaction probability. This phenomenon has been given several theoretical explanations [11-19]. However, also contradictory experimental results where no anomalous component is observed, have recently been presented [20-22].It is stressed in these reports that both systematic and statistical effects may simulate the anomalon effect. The importance of the choice of the mean-free-path estimator when the statistics get very low has particularly been pointed out in recent publications [23-24]. The combination of statistical and systematic errors are connected to the exact experimental conditions which are often complicated to

calculate. Here, we have developed a complete Monte Carlo program to simulate low statistics experiments. One emulsion experiment where the exact conditions are known to us [20,25] has been simulated. Several general conclusions concerning low statistics experiments can, however, be drawn from the simulations.

2. Simulation Input

Before introducing any anomalous fragments it is necessary to perform a simulation under fragmentation conditions as normal as the empirical knowledge allows. The various parts of the input that are introduced into the simulation is now described.

2.1. Finite Size Detector Effects

Geometrical effects may be of importance in a detector system where the fragment track length possible to follow will depend on the creation point and the direction of the fragment emission. The probability distribution $P_1(x,y)$ for the position of the entrance point (Fig.) is normally obtained directly from the exposed detector or from measurements during the irradiation. We should, however, stress here that an assumption of a uniform probability distribution within the scanned area is generally close enough to the actual $P_1(x,y)$ function. The the collision depth probability is given by:

$$P_2(z) = \lambda^{-1}\exp(-z/\lambda) \qquad (1)$$

where λ is the mean-free-path (mfp) of the beam nucleus in the detector. Naturally, the angular distribution of the beam nuclei must be considered if it cannot be assumed that all projectiles fall in perpendicular to the x,y plane.

2.2. Reaction Cross-Sections

In a mixed target medium - like emulsion or plastics - the mfp is:

$$\lambda = (\Sigma\ 1/\lambda_i)^{-1} = (\Sigma\ n_i\sigma_i)^{-1} \qquad (2)$$

where n_i stands for the number of i-target nuclei per volume unit and σ_i is the corresponding reaction cross-section. In general, it is necessary for the choice of the fragmentation distribution to simulate the identity of the target nucleus from the mfp branching ratio λ/λ_i. A well established description of the reaction cross-sections is given by the Bradt-Peters expression [26] with an overlap (transparency) term:

$$\sigma_i = \pi r_o^2\ (A_B^{1/3} + A_i^{1/3} - b)^2 \qquad (3)$$

where A_B is the beam nucleus mass.

With r_o=1.5 fm and b=1.3 formula (3) gives a good fit to all measured cross-sections. The $\lambda(A_B)$ curve for emulsions is shown in Fig. 2a. Due to an efficiency in the registration of events which is < 100% one would expect (3) to give shorter mfp:s than those measured in the experiment. However, since the particular experiment we are referring to [20] reports an ^{40}Ar mfp in emulsion of 8.97±0.16 cm as compared to 9.08 cm from (3) we use this parametrization in the subsequent simulations. Since the charge (and not the mass) of the secondary fragments are measured in emulsion experiments, we have assumed that the mass-distribution of fragments for each charge ($2 \leq Z \leq 18$) is of the general parabolic shape that was observed in fragmentation experiments [27]. The $\lambda(Z)$ function is shown in Fig. 2b. We should stress that any other reasonable mass distribution will not change the $\lambda(z)$ function to an extent which affects our conclusions in any way.

A simple mfp parametrization of the form;

$$\lambda = a\ Z^{-b} \tag{4}$$

has been suggested [1] and since this agrees well with the result shown in Fig. 2b, it is subsequently used. The smallest χ^2-value in a least squares fit is here found for a=27.5 fm and b=0.409.

2.3 Fragmentation Cross-Sections

The beam-, target- and fragment-mass (A_B, A_T and A_F) dependence of the relativistic fragmentation cross-sections has been described in terms of limiting fragmentation [28] or with the semi-empirical formula of Silberberg and Tsao [29]. None of these descriptions are general enough to cover all A_B, A_T, A_F-regions and therefore we have here adopted a simpler polinomial fit,

$$\sigma_F(Z) = A + BZ^d + CZ^e, \tag{5}$$

to existing fragmentat on cross-section data [28,30-31]. Fig. 3 shows a comparison with spectrometer data for $_{26}$Fe and $_8$O nuclei impinging on $_{47}$Ag and $_6$C targets. Generally, good fits are obtained for d=0.2 and e=0.8 when (5) is compared to the production of fragments with $A_F \geq A_B/2$. For lighter fragments the data is poor but a comparison with the Silberberg-Tsao formulae [29] (dashed histograms in Fig. 3) makes us believe that the same power law can be used generally.

The coefficients A, B and C are now individually determined in least squares fits to the experimental $\sigma(Z)$ functions for each projectile-target combination. The curve in Fig. 4 represents the result of this procedure for ^{40}Ar reactions in nuclear emulsions (charge interval $3 < Z_F < 18$). In fact, the final mfp results are rather insensitive to the choice of the $\sigma_F(Z)$ distribution. This is further discussed in section 5. It should be stated here, that the cross-section for the production of Z=2 fragments falls outside any standard parametrization, and the point in Fig. 4 for this charge is taken directly from empirical results.

2.4. Multifragmentation Channels

It should immediately be stated that there is very little empirical information about cross-sections for multi-fragmentation reaction channels. There are, however, some data from ^{16}O [32], ^{40}Ar [20] and ^{56}Fe [33] -induced reactions in nuclear emulsion, at least concerning the break-up into N_1 He-nuclei + N_2 $Z \geq 3$ fragments. The expected probabilities for various (N_1,N_2) channels as a function of Z_B are given in Table 1. In Fig. 5 the trend can be seen for the most populated $N_2=0$, $N_2=1$ and $N_2=2$ channels. In the $Z_B \geq 8$ region of projectiles the interpolation is well guided from the three ($Z_B=8$, 18, 26) data points, whereas for the lower Z_B region we have attempted to guide the (0,0) and (1,0) curves from break-up information of secondary He nuclei in the experiment of ref [20]. Because of the introduction of the multifragmentation channels we must modify the charge distribution from (5) in order to compensate for the non-available Z_F regions when $N_1 \geq 1$ or $N_2 \geq 2$. Since the highest charges will not be available when $N_2 \geq 1$ channels are introduced, the charge distribution will be affected in the following way:

$$f'(Z_F) = C \cdot \sum_{N_1=0}^{N_1,max} (W(N_1,1) \cdot P(N_1,Z_F))/f(Z_F) \qquad (6)$$

where

$$P(N_1,Z_F) = \begin{cases} f(Z_F)/(Z_B-2-2N_1) & \text{if } Z_F \leq Z_B-2N_1 \\ 0 & \text{if } Z_F > Z_B-2N_1 \end{cases}$$

where C is a normalization constant, $f(Z_F)$ is the inclusive charge distribution from (5) and $W(N_1,1)$ is the weight according to Table 1. Due to the small weights for $N_2 \geq 2$ channels these weights have been added to the corresponding $N_2 = 1$ channels. The aim is to reproduce $f(Z_F)$ after the introduction of the multifragmentation channels has been made. The compensation for heavy fragments with the inverse of $f'(Z_F)$ is, however, not sufficient (see open circles in Fig. 8). A stronger compenstation for the highest charges has therefore been introduced and in Fig. 4 the points show the result for the ^{40}Ar fragmentation from the Monte-Carlo simulation. The good agreement with

the inclusive distribution (curve) in this case makes us confident in using the same procedure also for $Z_B<18$, i.e. for later generations in the fragmentation chains.

2.5. Momentum Distributions

The projectile-like fragments from high energy nucleus-nucleus collisions have a dominant component, which is described in terms of a residual nucleus left from a sudden liberation of a number of Fermi gas nucleons [34]. A component with a harder $p_\perp$-spectrum has been observed at 2A GeV [35] but this is small enough to be neglected and thus we use Gaussian momentum (p_x, p_y) distributions as a consequence of the fragmentation process:

$$N(p_x)=\sqrt{\frac{2}{\pi}} \cdot \frac{1}{\sigma} \exp\left(-p_{x,y}^2/2\sigma^2\right) \qquad (7)$$

where the width is given as [34]:

$$\sigma^2=\sigma_0^2 \cdot A_F(A_B-A_F)/(A_B-1) \qquad (8)$$

The empirical values of σ_0 ranges from 70 to 90 MeV/c. Subsequently, we have used $\sigma_0=90$ MeV/c but neither a lower σ_0 with expression (7) nor any other suggested form of the A-dependence will affect the final results significantly.

2.6. Anomalons

The experiments which report on the observation of an anomalon component discuss a fraction of 2%-6% with a mfp of 2.5 cm. Since counter experiments [37] show that the lifetime of anomalons is $\gtrsim 10^{-10}$s and since it has been stressed [1] that the enhanced number of observed collisions is not directly due to decay-like events, we restrict our simulations to contain stable anomalons.

3. Simulation Scheme

The following procedure is adopted for the generation of a reaction chain (see also Fig. 1)

i) the position (x,y) of entrance is generated

ii) the depth of the primary collision is generated (if the beam nucleus stops or leaves the stack or a more restricted scanning volume, we register its length within the stack)

iii) the target identity is generated in case a target dependent fragmentation formalism [29] is adopted

iv) the charge and emission direction of all produced fragments with $Z \geq 2$ are generated (if an anomalon component is introduced, it is directly given $\lambda = 2.5$ cm)

v) the distance to the point where the fragment collides again or leaves the stack is generated

vi) all fragments are followed in all generations until the last $Z \geq 2$ fragment disappears.

The principal Monte-Carlo scheme is given in Fig. 6. A volume which corresponds to the emulsion stack is placed in a coordinate system with one corner at origo (Fig. 1). Beam particle (first generation particle) entrance coordinates (x,y) are generated from a uniform or empirical distribution. The restriction to the area A (Fig. 1) is made since no beam tracks too close to the edges are followed in the experiments.

The beam direction is (generally) assumed to be along the z-axis and the primary track length is now randomized following the standard uniform distribution function technique. Here, this means that the collision point is given by $z = -\lambda \cdot \ln(1-s)$ where λ is parametrized according to formula (3) and s is a random number uniformly

distributed in the interval (0,1). If z is less than the scanning depth the projectile collides, and the number of fragments emitted in the accepted forward cone of the collision (here $\theta \leq 10^{o}$) is given by the next random number, according to the probability functions of table 1. The charge is given from the compensated fragment distribution by the next random number, with the constraint that the total fragment charge must not exceed the charge of the fragmenting nucleus.

All secondary fragments are now treated with the following procedure: The direction is given by a genetrated $\vec{p}_{\perp}$-vector and the collision length is given from (1) with a λ value from (4). When the fragment is of generation 2 (i.e. emitted from a primary collision) the stop coordinates are directly given in the original coordinate system (see fragment F_3 in Fig. 1) whereas for fragments of later generations the new momentum vector $\vec{p}'$ is generated in a coordinate system with the z'-axis along the preceeding fragment direction (see e.g. fragment $F_{3,1}$ in Fig. 1). Thus $\vec{p}'$ must be transformed by rotation to the original system:

$$\boldsymbol{R} \cdot \begin{bmatrix} p'_x \\ p'_y \\ p'_z \end{bmatrix} = \begin{bmatrix} p_x \\ p_y \\ p_z \end{bmatrix} \qquad (9)$$

where

$$\boldsymbol{R} = \begin{bmatrix} \dfrac{\sqrt{p_y^2+p_z^2}}{p} & 0 & \dfrac{p_x}{p} \\ \dfrac{-p_x p_y}{p\sqrt{p_y^2+p_z^2}} & \dfrac{p_z}{\sqrt{p_y^2+p_z^2}} & \dfrac{p_y}{p} \\ \dfrac{-p_x p_z}{p\sqrt{p_y^2+p_z^2}} & \dfrac{-p_y}{\sqrt{p_y^2+p_z^2}} & \dfrac{p_z}{p} \end{bmatrix}$$

A collision is accepted if the collision point for the fragment (in the original system) is within the stack volume, otherwise the fragment has left the stack and the track length to the edge is calculated. All fragment data is stored before randomizing a new generation or a new primary .

Each generation of particles are generated in the same way, the only difference being the decreasing charge available for fragmentation. The chain is followed until no more Z≥2 fragments exist within the stack volume, whereafter a new primary is generated.

All simulations were performed on a NORD-500 computer where the random generator is initialized by the computer clock in the beginning of each simulated experiment. The mean number of random calls are 21 for each primary which gives $\sim 10^5$ random calls in each simulation. The random generator has been tested for 10^8 simulations, each time giving a new non-repeating random sequence.

4. Comparison with Experimental Results

The exact experimental conditions (no anomalons) of an ^{40}Ar+emulsion experiment [20,25] was introduced into our Monte-Carlo program and 600 simulations were performed. All output parameters will be statistically distributed with certain widths and in Fig. 7 we see e.g. how the number of Z=10 fragments (all generations) are distributed in experiments with a statistics of 100 to 3000 secondary interactions. The latter situation is representative for an emulsion experiment with "high" statistics [20] whereas a few hundred secondary interactions is typical for a "low" statistics experiment. In any case the width will introduce an error in any mfp parameter that is measured and this has to be considered in the evaluation of the results. For low statistics also the systematic error introduced by the bias of the mfp estimator must be considered. In Fig. 8 we show the behavior of the two suggested mfp estimators S/n_Z and $S/(n_Z+1)$ (S is the total track length which is followed). The points in Fig. 8 from our simulation do very well follow the analytical expressions given in [23,24], and thus confirm the problems with the estimator choice. In the statistical region (0-10 cm from the preceeding collision) where the experimental [20] and simulated number of Z=10 fragments per cm-bin lies (this region is marked by an arrow) it is obvious that the statistical fluctuations ($\pm$1 FWHM shown as error bars) are comparable to, or even smaller than, the difference between the estimator values. If the number of fragments per cm-bin decreases

from ~100 to ~50 there will be a systematic increase in the mfp of ~10% if the estimator S/n_z is used. The other estimator $S/(n_z+1)$, however, does not create any problem as long as the number of fragments is above ~50.

A normal way of increasing the statistics is to use a Z-parametrization of the mfp (4), and sum up the charge-independent mfp:s for several charges. In the experiment that we particularly consider here [20], this leads to a variation of the number of fragments per cm-bin as indicated by the second arrow in Fig. 8. Here, there will be no observable deviation from the normal mfp whichever estimator is used. Therefore, as long as no systematic error exists in the charge determination as a function of the distance from the collision point, it is desirable to enhance the statistics by collecting several charges, at least until the number of fragments per length interval exceeds a few hundred. It should be stressed that any way of dividing collected data into subgroups (e.g. smaller length bins, charge groups, intervals of scattering angles etc) will make the mfp estimator position move to the left in the graph of Fig. 8 and therefore increase the possibility to get critically large bias effects. Naturally this will also increase the statistical uncertainties in the mfp determination.

In ref. [20], as well as in most other experiments, the conclusions concerning anomalons are drawn from a $\lambda(x)$ plot (where x is the distance from the preceeding collision). In Fig. 9, we present such a plot for $3<Z<18$ fragments [20] of all generations. The charge independent normalized mfp Λ/λ_0 is used. The points are the experimental result, whereas the simulated statistical distribution of mfp:s in every second 1 cm-bin is presented as solid histograms. The average mfp value follows the horisontal $\Lambda/\lambda_0=1$ line very well and we therefore believe that the effects of the limited detector volume does not affect the normal behaviour significantly. We observe that the statistical distributions of the Λ/λ_0 parameter are, as expected, not symmetric around $\Lambda/\lambda_0=1$ but exhibit extended tails on the large $\Lambda/\lambda_0>1$-side.

In order to find with what significance an anomalous component (λ=2.5 cm) could be observed, we have also introduced a 2% (dotted histogram) and a 6% (solid histogram) contribution. In Fig. 10 we show the border lines for $<\Lambda/\lambda_0>$ $\pm$1 s.d. in these cases. For the 6% contribution we notice that i) the possibility to obtain Λ/λ_0=1.0 in the first bin is negligible and ii) the trend of the first few points should be significantly deviating from the Λ/λ_0=1.0 line. Thus we conclude that a 6% anomalon component, with the statistics used here, should be observable with high significance in emulsion experiments. With a 2% component, only the first point is on the average below the normal line by 1 s.d. Thus is such a contribution not observable in this emulsion experiment, and naturally emulsion experiments with lower statistics will have even greater difficulties in getting a significant result. For comparison, we show in Fig. 11 how the situation will be for 600 colliding primary Ar-nuclei. This corresponds to ~1000 primary Ar-nuclei in the scanning, which is a typical value for some published "low statistics" experiments. It is obvious that not even a 6% component will, in any way, be significantly observable with such statistics.

In some of the reports on anomalon observations, one is referring to an enhanced probability of reaction chains with several collisions [1]. We have performed (again 600) simulations for the Ar-experiment and the ratios between the number of collisions and the number of second generation fragments for the 2nd - 6th generation (until no $Z \geq 2$ fragments are left) are compared to data [25] in Table 2. Naturally, the finite geometry of the detector will be very important in this case. The data in Table 2 is therefore selected from the total data in the experiment [25] in such a way that scanning and measurement conditions are the same as in the simulation. It is obvious that the experimental result shows no significant deviations from what is expected for a normal fragmentation procedure, in agreement with the statements about the $\lambda(x)$ results in [20]. The possibility to obtain significant results with a 2% or 6% anomalon component is tested. The largest chain probabilities are obtained if full memory of the anomalous effect is adopted. We observe in Table 2 a dramatically enhanced probability for chains with many generations and conclude that this is significant already for three generations. In the 5:th

generation (F_5), the expected anomalon signal is very clear. The probability to obtain such chains in one single experiment is however small, a fact which is confirmed by the results of the experiment [25] which is used as reference.

4. Systematic Errors

It has been the main purpose of this paper to discuss the statistical significance of anomalon experiments. In the simulations there is, however, also introduced the systematic errors which may come from the finite detector geometry. Other kinds of systematic errors may appear and we discuss some of them here, particularly those which can be tested by introducing them into the Monte-Carlo simulation program.

i) The fragmentation charge distribution (5) may be incorrectly measured for some reason. This will of course affect the mfp estimations, and possibly the ratio between the Z-independent mfp for various generations. In order to test an extreme case, we introduced $\sigma_p(Z)$=constant in the available Z-region for each collision (all generations) into the simulation. The conclusion of this test is that nothing in the $\lambda(x)$ or chain results will be enough affected to change any conclusions about the anomalon component.

ii) Changing the width of the p_t distribution (7) of fragments from σ_0 = 90 MeV/c to σ_0 = 70 MeV/c or the introduction of a harder fragmentation component according to ref [35] does not change any conclusion significantly.

iii) The confusion from collisions of "low energy" Z=1 particles with the same dE/dx close to the preceeding collision as heavier projectile-like fragments has been discussed in ref [25]. This effect may introduce a number of false collisions, which is decreasing rapidly with the distance from the preceeding collision point. The calculated effect gives a 45% decrease in

Λ/λ_0 [25] for the first 1 cm bin for all fragments with $3 \leq Z \leq 5$. This is hardly enough to create the "anomalon effect" and it will be further reduced as soon as one introduces any criteria on the topology of a high energy collision.

iv) The confusion due to interactions of high energy Z=1 or neutron collisions, within a cylinder around the heavy fragment where spatial separation of vertices cannot be obtained, has also been calculated. The effect has a similar distance dependence as iii) and is of the same importance. However, in this calulation it was assumed that only the light particles have a realistic angular distribution while the fragment has $\theta=0^0$. We have now performed a test with the Monte-Carlo program, where this confusion-component is introduced (λ=35 cm). With $\theta=0^0$ for fragments it confirms the importance of the effect, but when introducing realistic angular distributions both for fragments and light particles the confusion effect has decreased to such an extent that it becomes completely negligible.

v) Other possible systematic errors introduced by measurement techniques, inhomogenity in the detector material , energy variation of cross-sections, differential scanning efficiencies or hyperfragment decays have been carefully investigated in ref [1], and none of them is there found to give any significant contribution to the anomalon effect.

Conclusions

The Monte Carlo simulations of fragmentation chains in emulsion experiments show that a 2% anomalon component cannot be significantly observed, mainly due to statistical fluctuations. A 6% component should be observed from significantly lower mfp:s within 3 cm from the preceeding collision or from chain probabilities. For experiments with essentially lower statistics than the one discussed here (3000 interacting primaries), it is confirmed that the choice of the estimator is important. The indications of an anomalon component in some emulsion experiments may be a combination of statistical and

systematic effects (in particular the confusing from low energy Z=1 particles should be considered). We stress here that we have only been able to simulate one experiment, with negative result concerning anomalons, since experimental conditions must be known. The program is however general enough to be able to simulate other experiments on request to the authors.

We thank Dr S Garpman for several detailed discussions about the Monte Carlo program. The Banaras-Chandigarh-Jammu-Jaipur-Lund Collaboration is acknowledged for allowing us to use reaction chain data prior to publication.

References

1. E M Friedlander et al, Phys Rev Lett 45(1980)1084 and Phys Rev C27(1933)1489

2. P L Jain and G Das, Phys Rev Lett 48(1982)305

3. H B Barber, P S Freier and C J Waddington, Phys Rev Lett 48(1982)856

4. M El-Nadi et al, Phys Rev Lett 52(1984)1971

5. E Ganssauge et al, Proc of the 7th High Energy Heavy Ion Study, GSI 1984 p 593, editors R Bock, H H Gutbrod and R Stock

6. D Ghosh et al, Proc of the 7th High Energy Heavy Ion Study, GSI 1984 p 661, editors R Bock, H H Gutbrod and R Stock

7. C N Agakishiev et al, JINR-preprint P1-82-795, Dubna 1982

8. A P Gasparian and N G Grigalashoili, Proc 10th Int Conf on Particles and Nuclei, Heidelberg 1984, Vol II, p 218

9. M L Tincknell, P B Price and C J Waddington, Phys Rev Lett 51 (1983) 1948.

10. G Dersch et al, Proc of the 7th High Energy Heavy Ion Study, GSI 1984, p 599 and
Proc of the Second Int Conf on Nucleus-Nucleus Collisions, Visby, Sweden 1985, p 180 in volume I.

11. Y Karant and M H McGregor, Phys Rev Lett 50(1983)215

12. W J Romo and P J Watson, Phys Lett 88B(1979)354

13. S Fredriksson and M Jändel, Phys Rev Lett 48(1982)14

14. J Boguta, Phys Rev Lett 50(1983)148

15. G F Chapline, Phys Rev D25(1982)911

16. P J S Watson et al, Phys Rev D27(1983)1468

17. B F Bayman, P S Ellis and Y C Tang, Phys Rev Lett 49(1982)532

18. Y E Kim and M Orlowski, Phys Lett 140B(1984)275 and Phys Rev C29(1984)2299

19. I N Mishustin, The Niels Bohr Institute Preprint NBI 84-14, 1984

20. R Bhanja et al, Phys Rev Letters 54(1985)771

21. G Baroni et al, Nucl Phys A437, (1985) 729

22. W Heinrich et al, Phys Rev Lett, 52(1984)1401

23. E S Pshenin and V G Voinov, Phys Lett 128B(1983)13

24. S Garpman et al, Phys Rev Lett 53(1984)2195

25. Banaras-Chandigarh-Jaipur-Jammu-Lund Collaboration

26. H L Bradt and B Peters, Phys Rev 77(1950)54

27. D E Greiner et al, Phys Rev Lett 35(1975)152

28. G D Westfall et al, Phys Rev C19(1979)1309

29. R Silberberg and C H Tsao, Proc of the 15th Int Cosmic Ray Conference, Plovdiv 1977 Vol 2, p 89

30. P J Lindstrom et al, Lawrence Berkeley Laboratory Report LBL-3650, 1975

31. Y P Viyogi et al, Phys Rev Lett 42(1979)33

32. C Bjarle et al, Nucl Phys A381(1982)544

33. K B Bhalla, S Lokanathan and Y Prakash, private communication

34. A S Goldhaber, Phys Lett 533(1974)306

35. B Jakobsson, R Kullberg and I Otterlund, Lett al Nuovo Cimento 15(1976)444

36. H A Gustafsson et al, Phys Rev Lett 51(1983)363

Figure Captions

1. The geometry of a simulated fragmentation chain. A is the accepted entrance area in the x,y plane. F_3 stands for the 3rd fragment in the 2nd generation, $F_{3,1}$ for the 1st fragment in the 3rd generation etc. $\hat{z}$ denotes the preceeding fragment direction. The notations ● and o stand for the points where the fragments either leave the stack, or are lost because no $Z \geq 2$ fragment is emitted in the collision.

2. Mean-free-path in emulsion for high energy ($E/A \gtrsim 0.5$ GeV) nuclei as a function of the mass number (2a) or charge number (2b). The underlying formulae are given in the text.

3. Histograms show experimental fragmentation charge distributions (solid) or distributions based on semi-empirical formulae (dashed) [19]. The points are the results of the adopted polinomial fit.

4. The experimental fragmentation charge distribution for ^{40}Ar induced collisions in emulsion [20] (histogram) compared to the Monte Carlo simulated results (black points). The curve is the direct result of formula (5). The open points are explained in the text.

5. Multifragmentation channel probabilities, as a function of the projectile charge. (N_1,N_2) stands for the channel with N_1 He-nuclei and N_2 $Z \geq 3$ fragments. The sum of the probabilities for all (N_1,N_2) channels for each projectile charge (including those not presented in the figure) is unity.

6. The Monte Carlo computer scheme for simulation of fragmentation chains in track detectors.

7. Statistical (Monte Carlo simulated) distributions of the number of generated Z=10 fragments for experiments where 100, 300, 600, 1700 and 3000 secondary interactions are recorded. The original collision is for ^{40}Ar in nuclear emulsion at 1.8A GeV.

8. The estimated mfp (s/n_Z and s/n_Z+1) of Z=10 fragments, normalized to the normal mfp $(\lambda_0)_Z$ as a function of the number of generated Z=10 fragments. The curves are the results of the analytic derivation from ref [24] and the points (with errors within the points) are from this Monte Carlo simulation. The error bars represent the FWHM width of the n_Z distributions of Fig. 7. The black arrows show the regions of statistics for Z=10 and $3 \leq Z \leq 18$ fragments in the various cm-bins, as they are presented in refs [20,25].

9. Charge independent normalized mfp Λ/λ_0-distributions as a function of distance from the collision point is shown as histograms for no anomalon component (solid histogram), for a 2% (dotted histogram) and 6% (dashed histogram) contribution. The dots show the experimental results [20].

10. $\langle \Lambda/\lambda_0 \rangle \pm 1$ s.d. borderlines as a function of distance is shown for histograms from Fig. 9.

11. Charge independent normalized mfp Λ/λ_0-distributions as a function of distance from the collision point for 600 colliding primary Ar-nuclei. Solid histograms have no anomalous component, dashed histogram has a 6% contribution.

Table 1. Probabilities for multifragmentation channels with N_1 He and N_2 $Z \geq 3$ fragments in a reaction of a projectile with charge Z_B in nuclear emulsion. All channels with a probability < 0.005 have been left out.

								PROBABILITY								
(N_1,N_2)	Z_B= 2	3	4	5	6	7	8	9	10	11	12	13	14	15	16	17	18
0,0	.72	.69	.65	.49	.45	.38	.35	.30	.26	.23	.20	.17	.15	.13	.12	.11	.10
1,0	.28	.31	.31	.24	.22	.19	.17	.16	.14	.13	.12	.11	.10	.10	.09	.08	.08
2,0				.14	.14	.13	.12	.11	.10	.09	.09	.08	.08	.07	.07	.06	.06
3,0						.07	.08	.08	.07	.07	.06	.06	.05	.05	.05	.04	.04
4,0								.01	.01	.01	.02	.02	.03	.03	.03	.03	.03
5,0												.01	.01	.01	.01	.01	.01
0,1			.04	.13	.18	.20	.22	.24	.25	.26	.26	.26	.27	.27	.28	.28	.28
1,1					.01	.03	.06	.09	.11	.13	.14	.15	.16	.17	.18	.18	.18
2,1							.01	.03	.05	.07	.08	.09	.10	.11	.11	.11	.12
3,1										.01	.02	.03	.04	.04	.05	.05	.05
0,2											.01	.01	.01	.02	.02	.02	.03
1,2															.01	.01	.01
2,2																	.01

Table 2. Reaction-chains from experiment and simulations. F_1 is the number of particles in the first fragment generation and F_1^* is the number of colliding fragments ($Z \geq 2$) for this generation etc. The ratio F_N^*/F_1 is taken for all fragment generations.

	Experiment	Simulation no anomalons	Simulation 6% anomalons, full memory
F_1	2152	2147.7	2150.5
F_1^*	921	1021.5	1132.4
F_1^*/F_1	0.430 ± 0.017	0.476 ± 0.001	0.527 ± 0.001
F_2^*	154	172.4	258.5
F_2^*/F_1	$(7.16 \pm 0.60) \cdot 10^{-2}$	$(8.03 \pm 0.03) \cdot 10^{-2}$	$(12.0 \pm 0.03) \cdot 10^{-2}$
F_3^*	20	15.7	42.8
F_3^*/F_1	$(9.29 \pm 2.09) \cdot 10^{-3}$	$(7.31 \pm 0.08) \cdot 10^{-3}$	$(19.9 \pm 0.13) \cdot 10^{-3}$
F_4^*	2	0.95	5.92
F_4^*/F_1	$(9.29 \pm 6.57) \cdot 10^{-4}$	$(4.42 \pm 0.19) \cdot 10^{-4}$	$(27.5 \pm 0.46) \cdot 10^{-4}$
F_5^*	-	0.05	0.69
F_5^*/F_1	-	$(2.48 \pm 0.44) \cdot 10^{-5}$	$(32.1 \pm 1.58) \cdot 10^{-5}$
F_6^*	-	-	0.066
F_6^*/F_1	-	-	$(30.7 \pm 4.88) \cdot 10^{-6}$

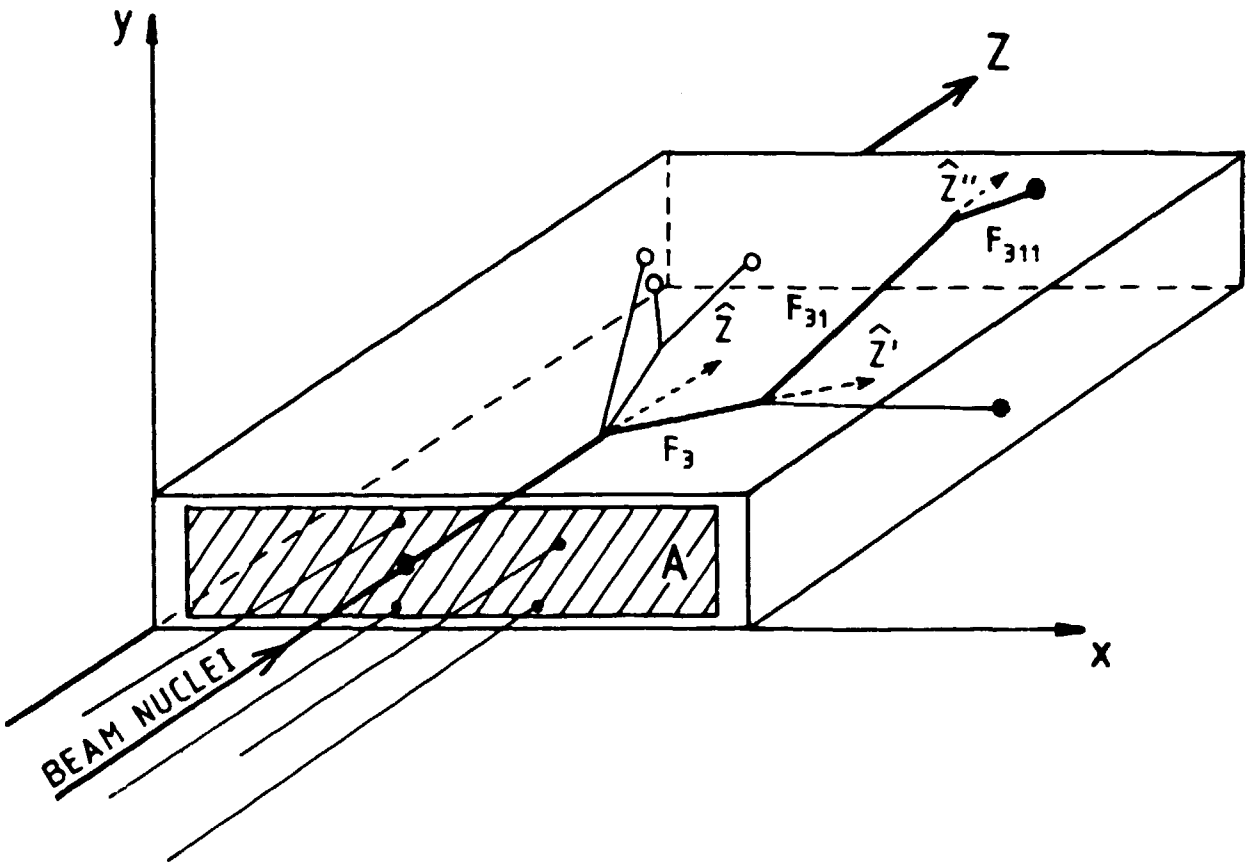

FIG 1

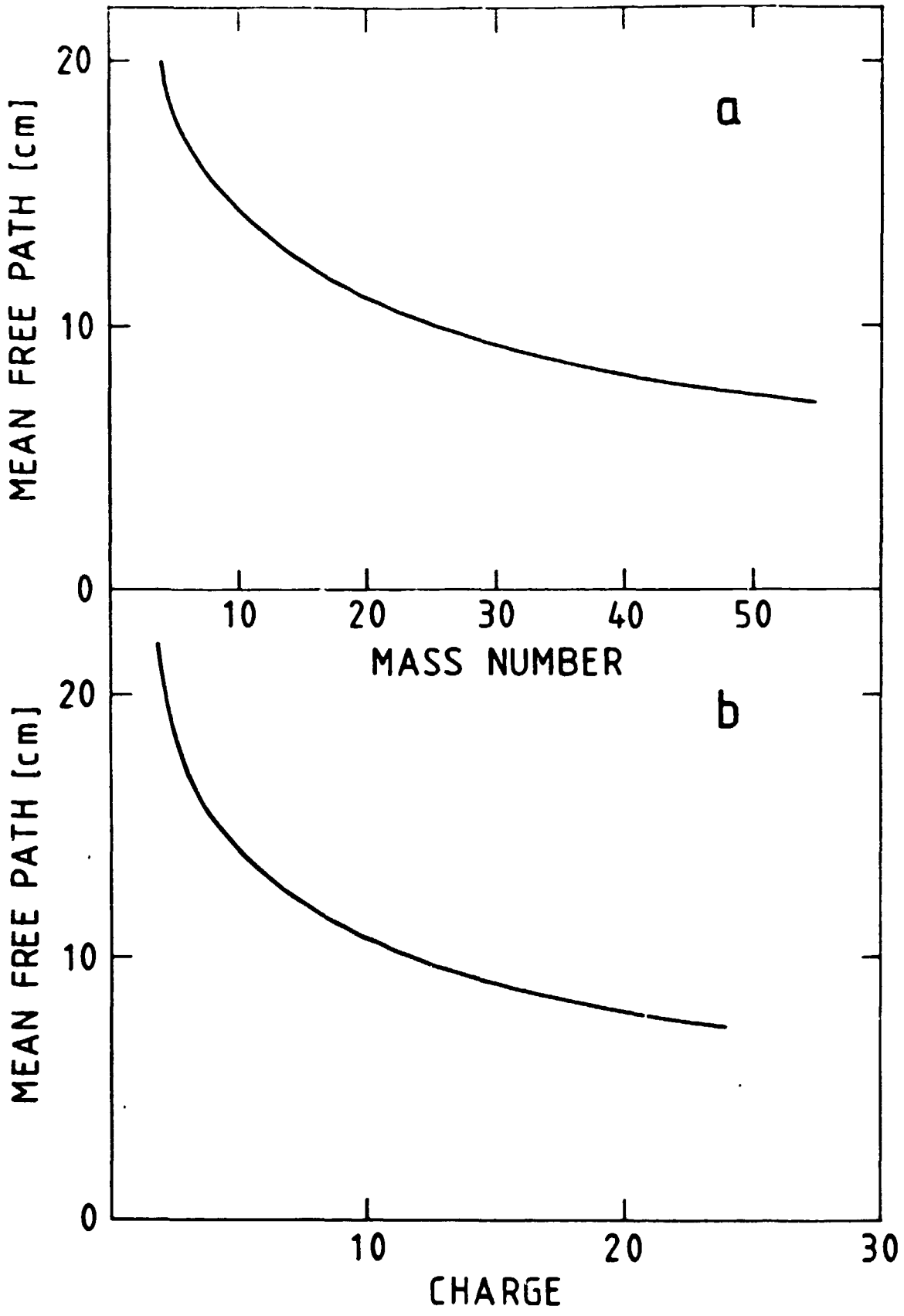
a
MEAN FREE PATH [cm]
20
10
0
10
20
30
40
50
MASS NUMBER
b
MEAN FREE PATH [cm]
20
10
0
10
20
30
CHARGE

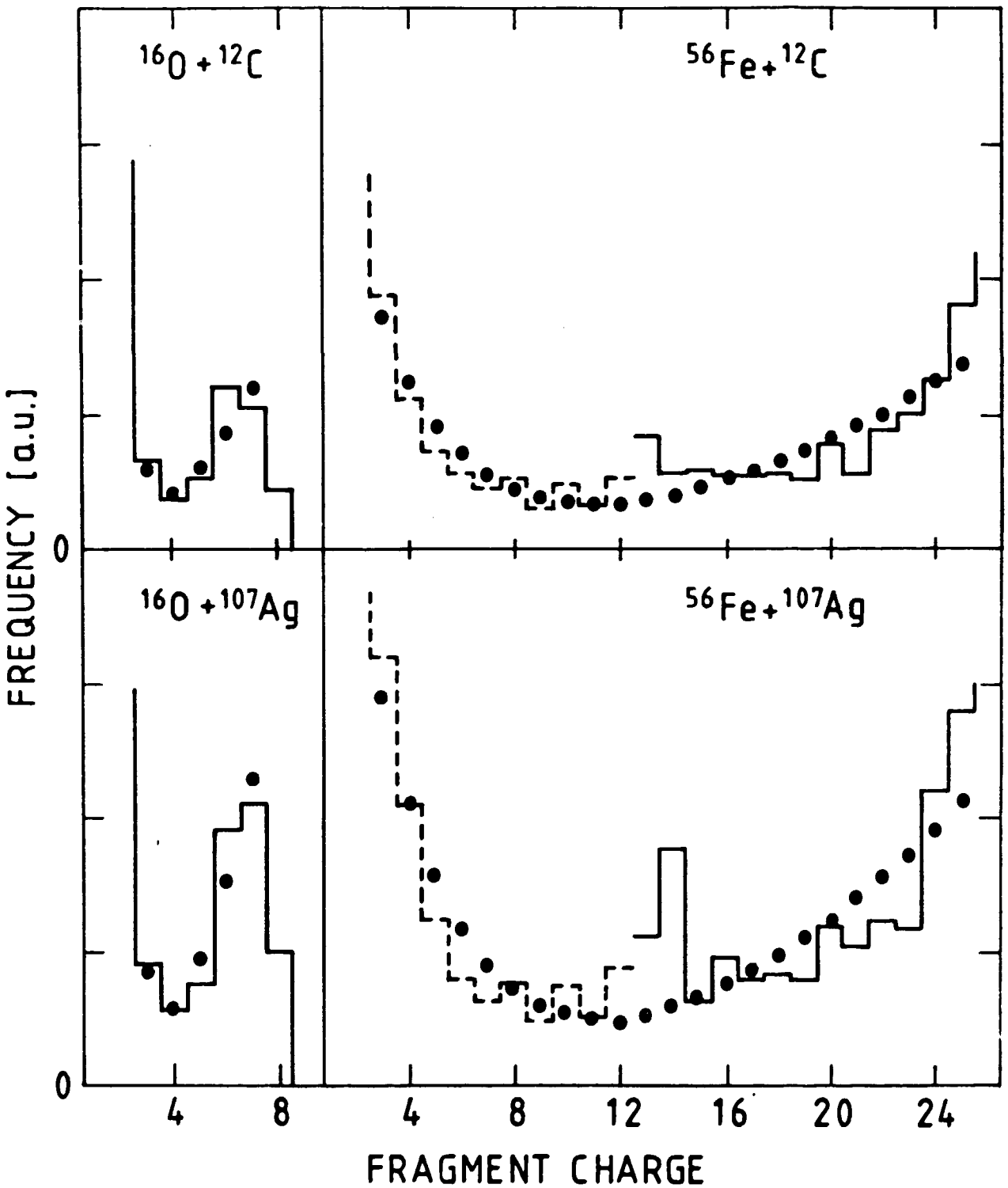
$^{16}O + ^{12}C$
$^{56}Fe + ^{12}C$
$^{16}O + ^{107}Ag$
$^{56}Fe + ^{107}Ag$
FREQUENCY [a.u.]
0
0
4
8
4
8
12
16
20
24
FRAGMENT CHARGE

Fig 3

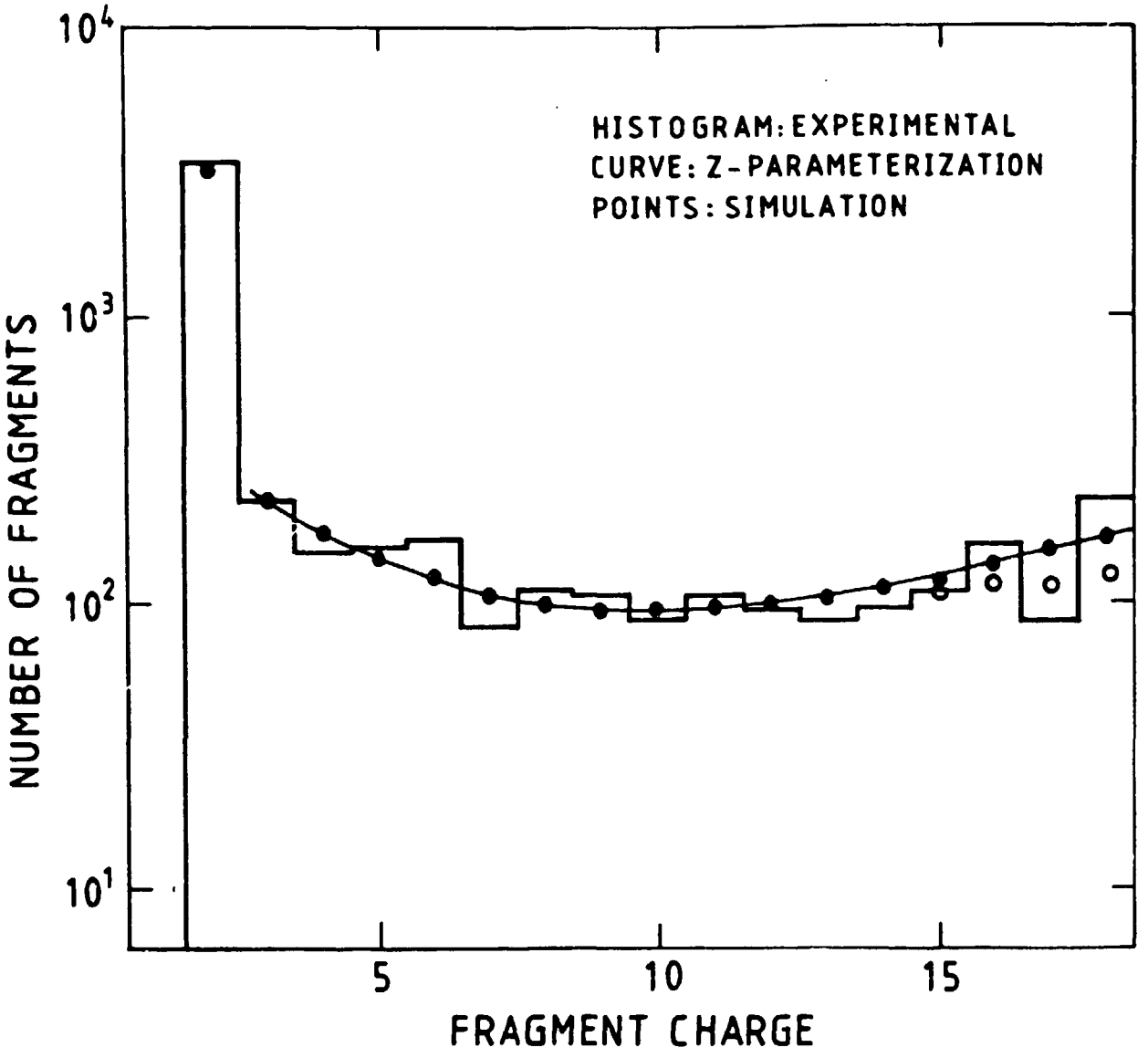
HISTOGRAM: EXPERIMENTAL
CURVE: Z-PARAMETERIZATION
POINTS: SIMULATION
NUMBER OF FRAGMENTS
10^4
10^3
10^2
10^1
5
10
15
FRAGMENT CHARGE

Fig 4

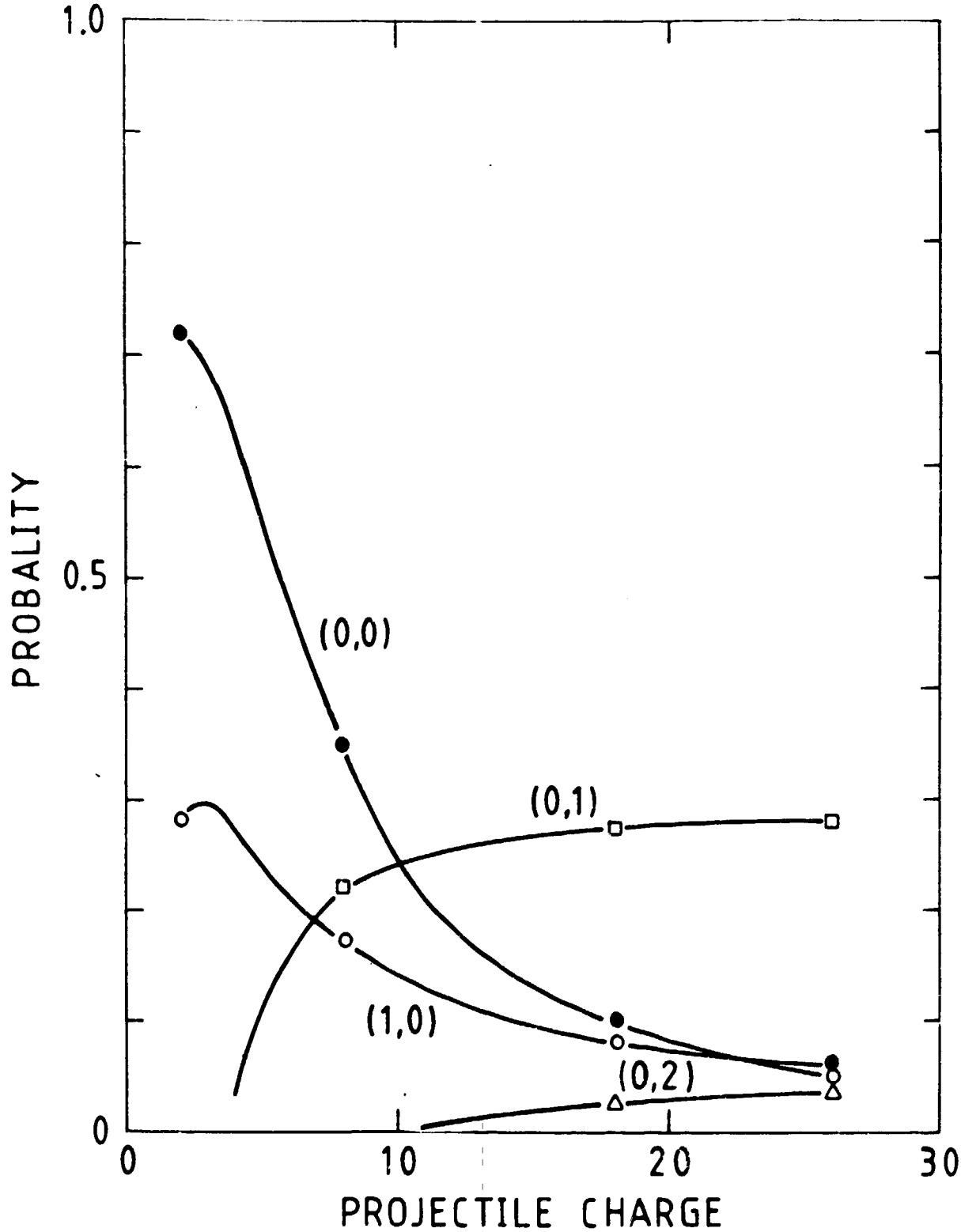

FIG 5

F L O W - C H A R T

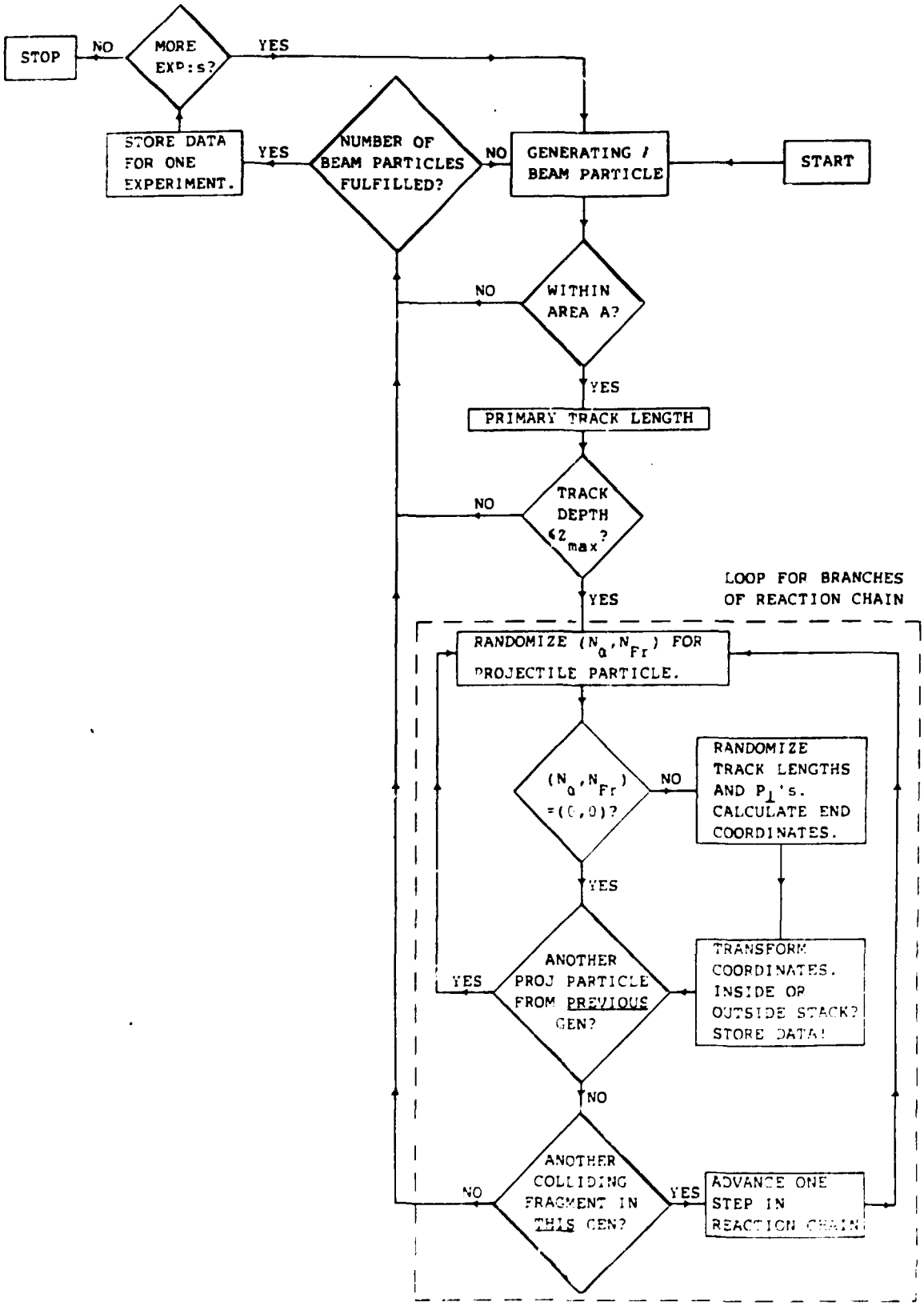

FIG 6

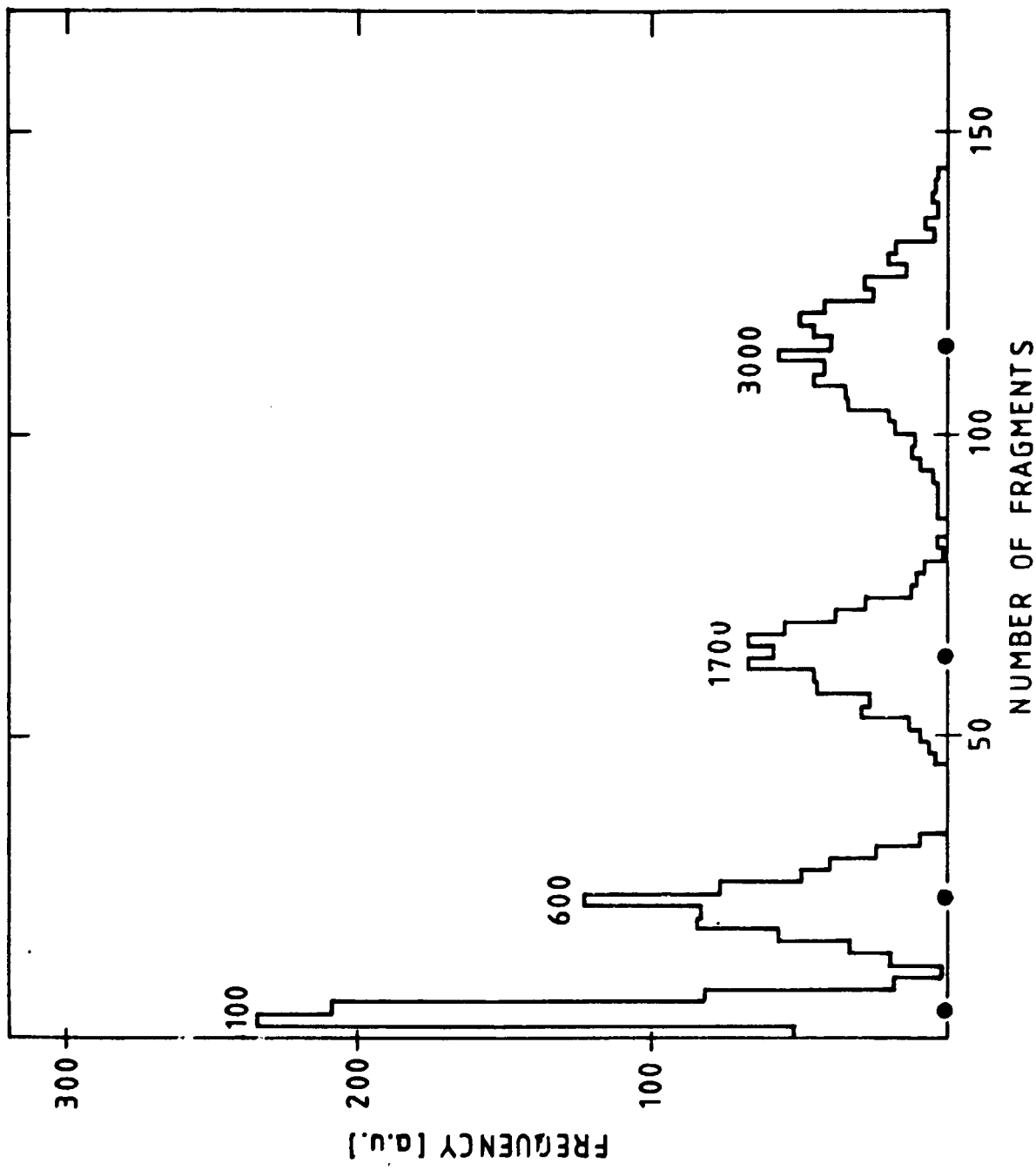
FREQUENCY [a.u.]
300
200
100
100
600
170u
3000
50
100
150
NUMBER OF FRAGMENTS

Fig 7

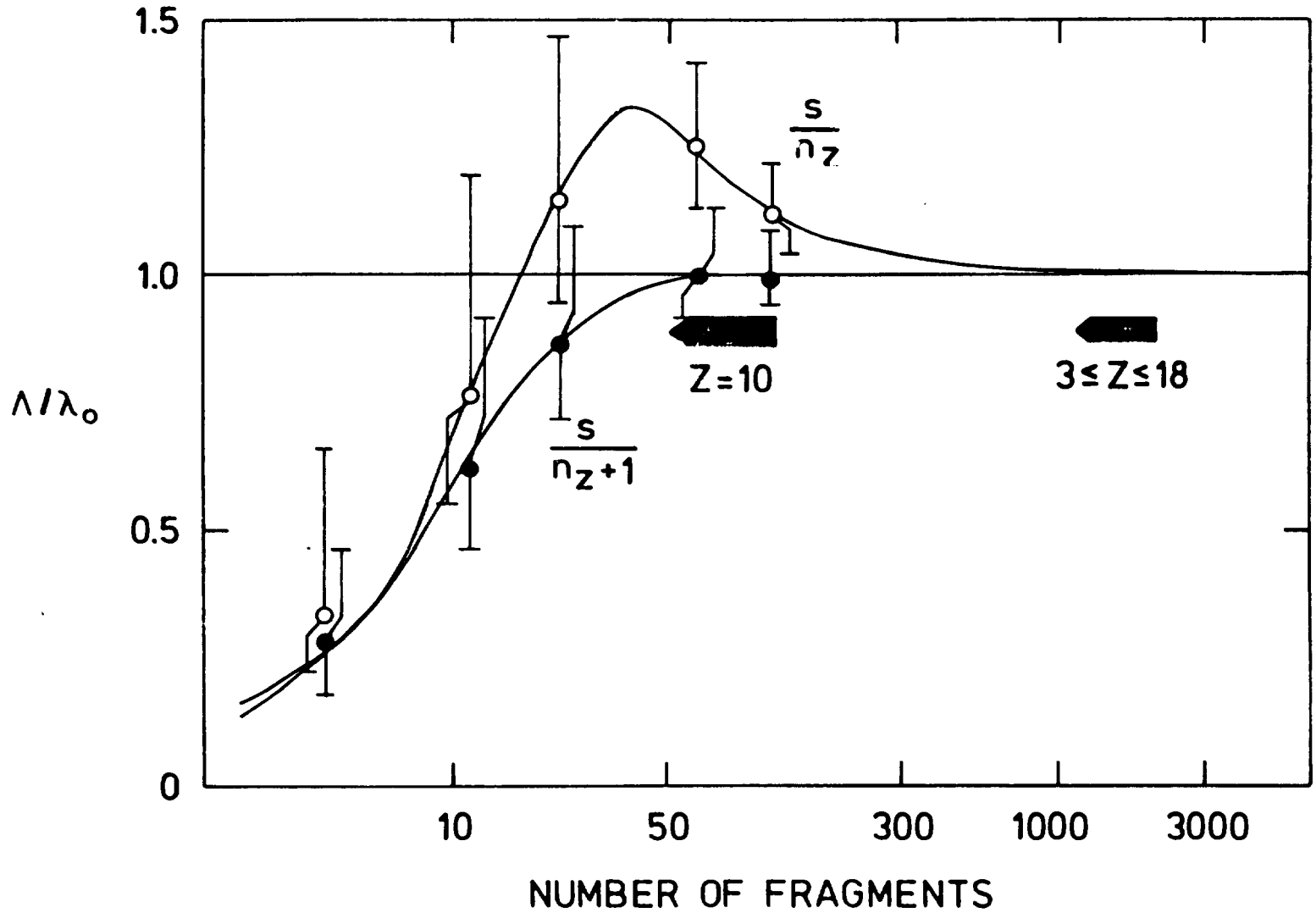
1.5
1.0
0.5
0
Λ/λo
s/nz
s/nz+1
Z=10
3≤Z≤18
10
50
300
1000
3000
NUMBER OF FRAGMENTS

Fig 8

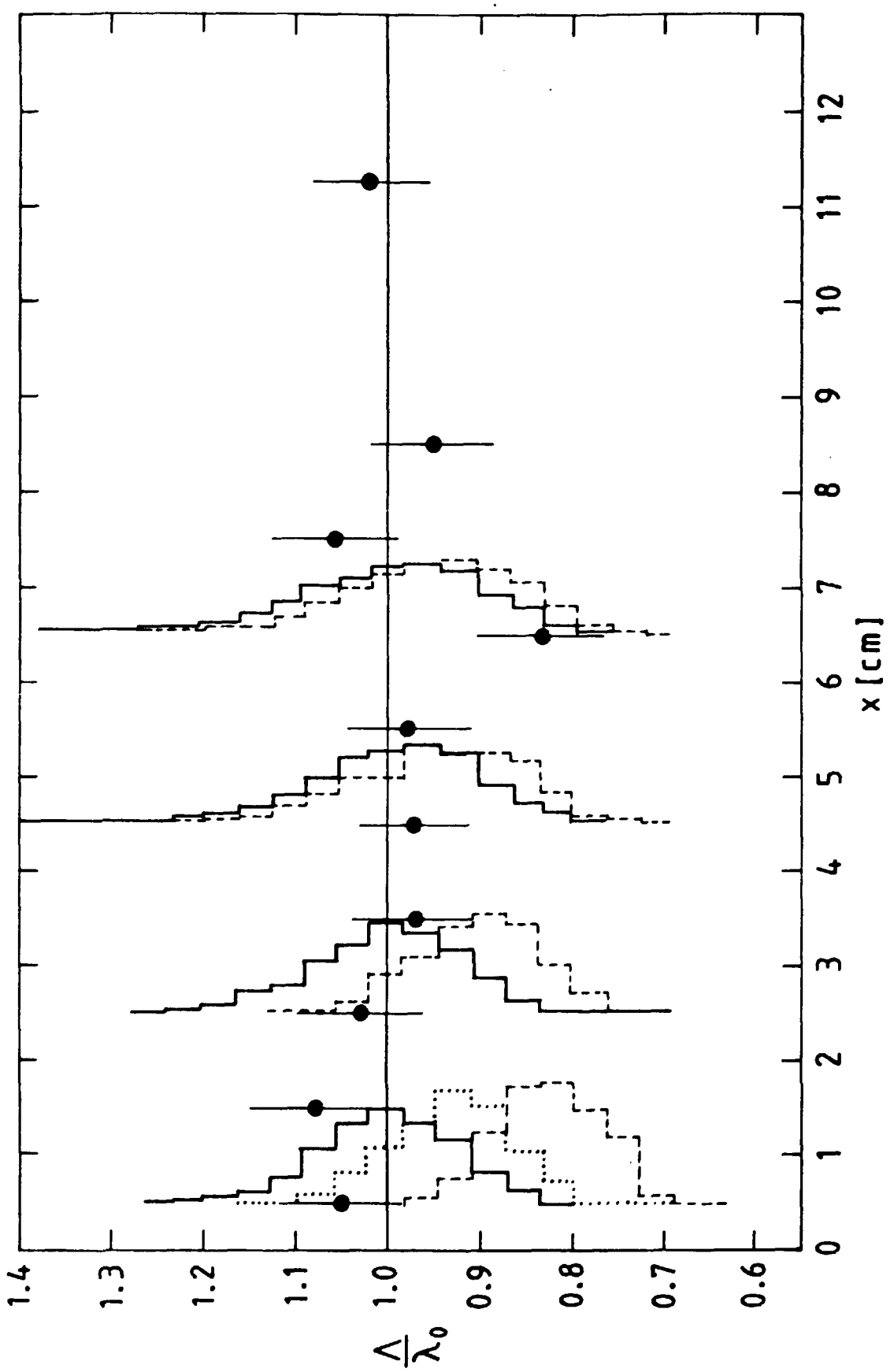
1.4
1.3
1.2
1.1
1.0
0.9
0.8
0.7
0.6
$\frac{\Lambda}{\lambda_0}$
0
1
2
3
4
5
6
7
8
9
10
11
12
x [cm]

FIG 9

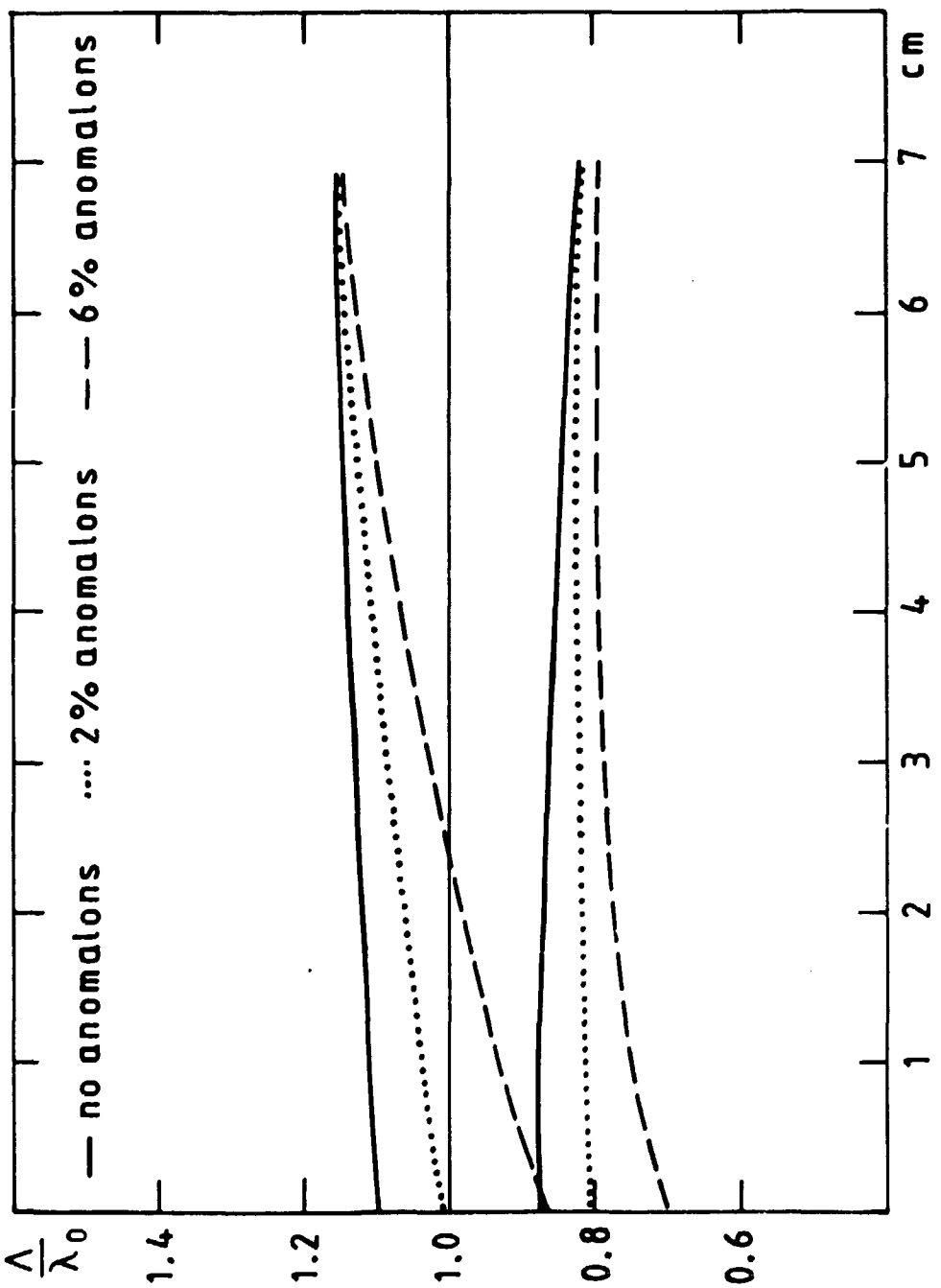
— no anomalons
···· 2% anomalons
– – 6% anomalons
$\frac{\lambda}{\lambda_0}$
1.4
1.2
1.0
0.8
0.6
1
2
3
4
5
6
7
cm

FIG 10

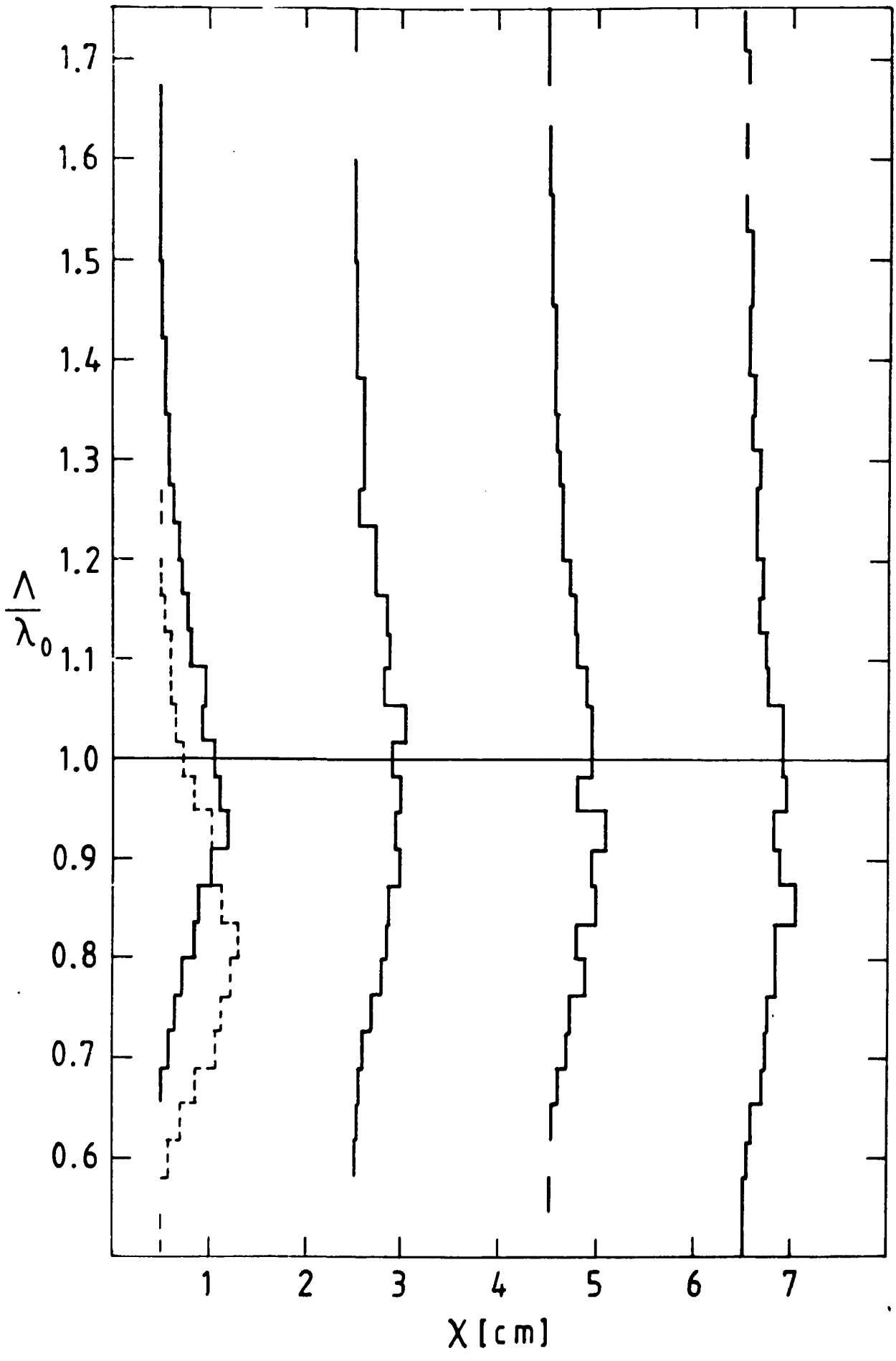

FIG 11

TYP AV DOKUMENT	DOKUMENTBETECKNING/CODEN
☐ Doktorsavhandling ☐ Rapport ☐ Tidskriftsartikel ☐ Examensarbete ☐ Delrapport ☐ Konferensuppsats ☐ Kompendium ☐ Slutrapport ☒ INTERNRAPPORT	LUIP8512 LUNFD6/(NFFK-7065)

AVDELNING/INSTITUTION
Division of Cosmic and Subatomic Physics, University of Lund,
Sölvegatan 14, S-223 62 LUND, Sweden

FÖRFATTARE
Norén, Birgitta and Jakobsson, Bo

DOKUMENTTITEL OCH UNDERTITEL
Monte-Carlo Simulations of Anomalon Experiments

SAMMANFATTNING

Computer simulations of low statistics track detector heavy ion collision experiments on projectile fragmentation are presented. We find a non-negligible probability to obtain the recently observed anomalous fragmentation component also with normal fragmentation processes. We discuss the significance of the expected mean-free-path behaviour when an anomalous component is included.

NYCKELORD heavy ion collision, mean-free-path, secondary fragment, significance, anomalous fragmentation

DOKUMENTTITEL OCH UNDERTITEL – SVENSK ÖVERSÄTTNING AV UTLÄNDSK ORIGINALTITEL
Monte-Carlo simulering av anomalonexperiment

TILLÄMPNINGSOMRÅDE
Programmet simulerar lågstatistikexperiment av fragmentering i tungjonskollisioner

NYCKELORD tungjonskollisioner, fragmentering, simulering, normalkomponent, anomalkomponent

UTGIVNINGSDATUM	ANTAL SID (inkl bilagor)	SPRÅK
år 86 mån 01	31	☐ svenska ☒ engelska ☐ annat

ÖVRIGA BIBLIOGRAFISKA UPPGIFTER

ISSN 0348-9329
ISBN
PRIS

I, the undersigned, being the copyright owner of the abstract, hereby grant to all reference sources permission to publish and disseminate the abstract.

Mottagarens accessionsnummer

Date: Lund 850114

Signature: Birgitta Norén